Multimodal PDMS triboelectric nanogenerator sensor based on anodised aluminium oxide template preparation for object recognition

Hongde Zhu, [a] Junlan Liang, [b] Sanlong Wang, [c] Junjun Huang, [**bc] Zhenming Chen[*abc]

[a] School of Materials Science and Engineering, Guilin University Of Electronic Technology, Guilin City, 541004 China

[b] Guangxi Key Laboratory of Calcium Carbonate Resources Comprehensive Utilization, College of Materials and Chemical Engineering, Hezhou University, Hezhou City, 542899, China

[c] School of Chemistry and Chemical Engineering, Hefei University, Hefei City, 230009, China

Corresponding Authors: *Zhenming Chen   E-mail: chenzhenming2@163.com

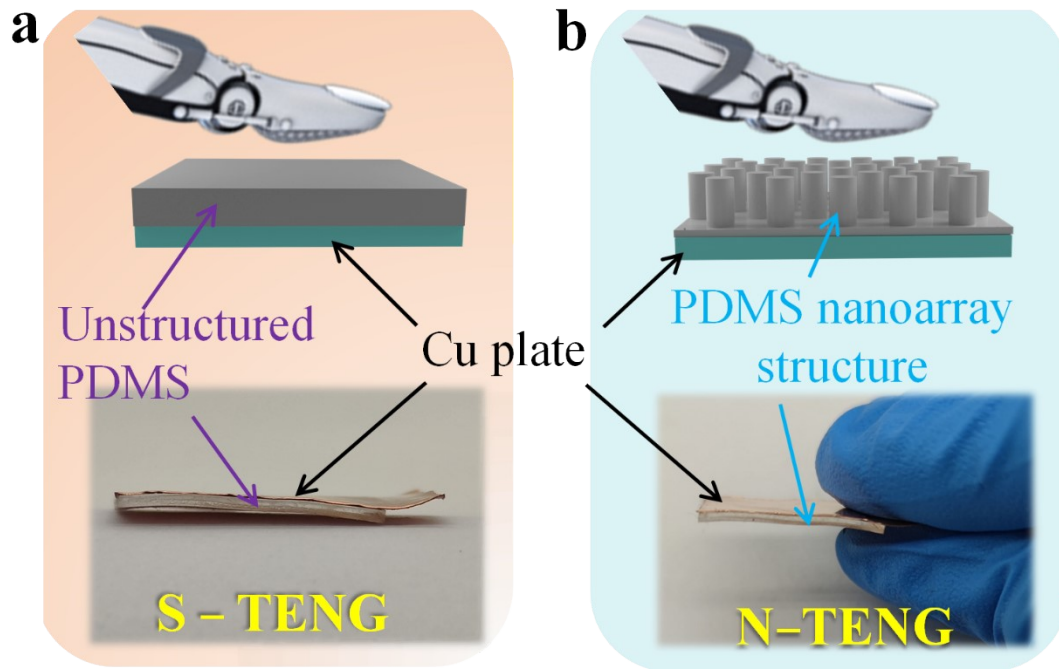   ** Junjun Huang   E-mail: huangjunjun163@163.com

Fig. S1. Structural diagram and optical photograph of S-TENG (a) and N-TENG (b) devices.

Fig. S1 shows the structure diagram of the S-TENG and N-TENG equipment. The PDMS side of the N-TENG triboelectric material has a nano-columnar structure prepared by a template combined with ultrasound technology, and the smooth surface is bonded with the Cu plate (Fig. S1a). To further verify the unique characteristics of the N-TENG device, we made a conventional TENG device in single-electrode mode. Assembly of friction nanogenerators (S-TENG) was achieved by bonding PDMS without nano-array structures onto copper plates (Fig. S1b). In this work, the thickness of the two devices was 0.07 cm.
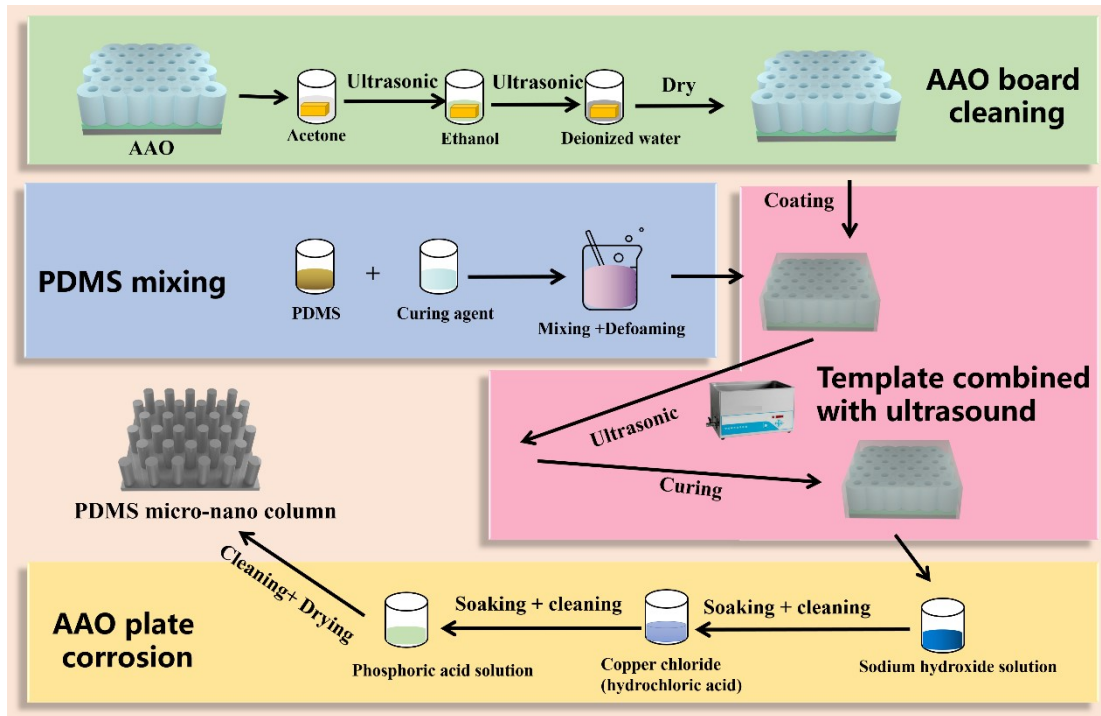
Fig. S2. Schematic diagram of the fabrication process of the N-TENG device.

AAO template cleaning: Owing to the small aperture (300 nm) of AAO, it easily attracts dust in the air, blocks the hole cavity, and retains debris at the edge of the plate during cutting. Thus, it is necessary to clean the AAO plate before use. The AAO plate was placed into acetone, ethanol, and deionised water for ultrasonic cleaning for 10 min. After cleaning, the AAO plate was placed into a vacuum drying oven for drying at 50°C and set aside.

PDMS mixing: Before the experiment, the PDMS prepolymer and curing agent were weighed at a mass ratio of 10:1, mixed fully, and then put into a 0.06 MPa vacuum box for 30 min to defoam.

Template combined with ultrasound: The thoroughly mixed and defoamed PDMS (the mass ratio of prepolymer and curing agent was 10:1) was coated on the cleaned AAO and allowed to stand for 10 min. After the surface was naturally levelled, it was placed into a 24 kHz ultrasonic instrument for 30 min. Then, the plate was removed, the excess PDMS on the edge of the plate was wiped off, and finally, the plate was placed into an 85°C oven for curing for 1.5 h.

AAO template corrosion: After ultrasonic treatment, the plate was placed into an 85°C air drying oven for curing for 1.5 h. After curing, the plate was placed into 4 mol/L

sodium hydroxide, saturated copper chloride solution, and 5% phosphoric acid solution to completely corrode and dry to obtain a PDMS film with a nano-columnal structure on the surface.
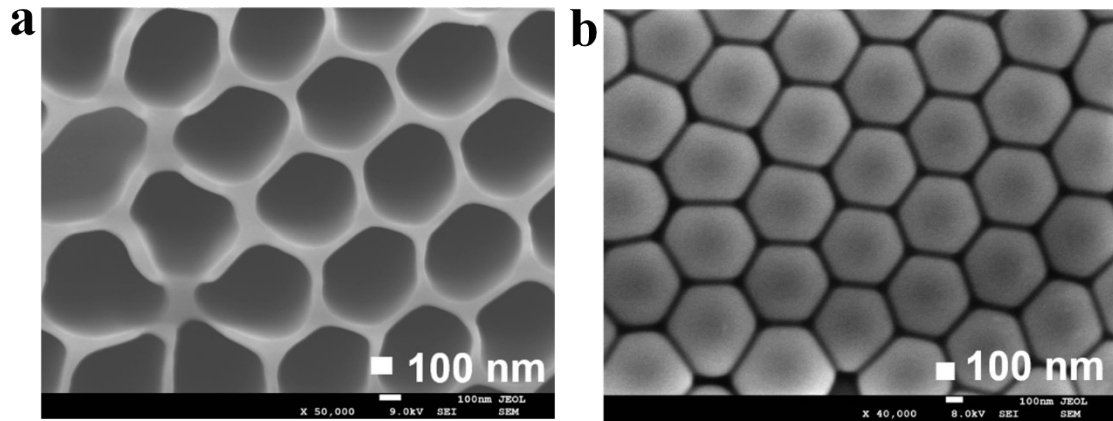

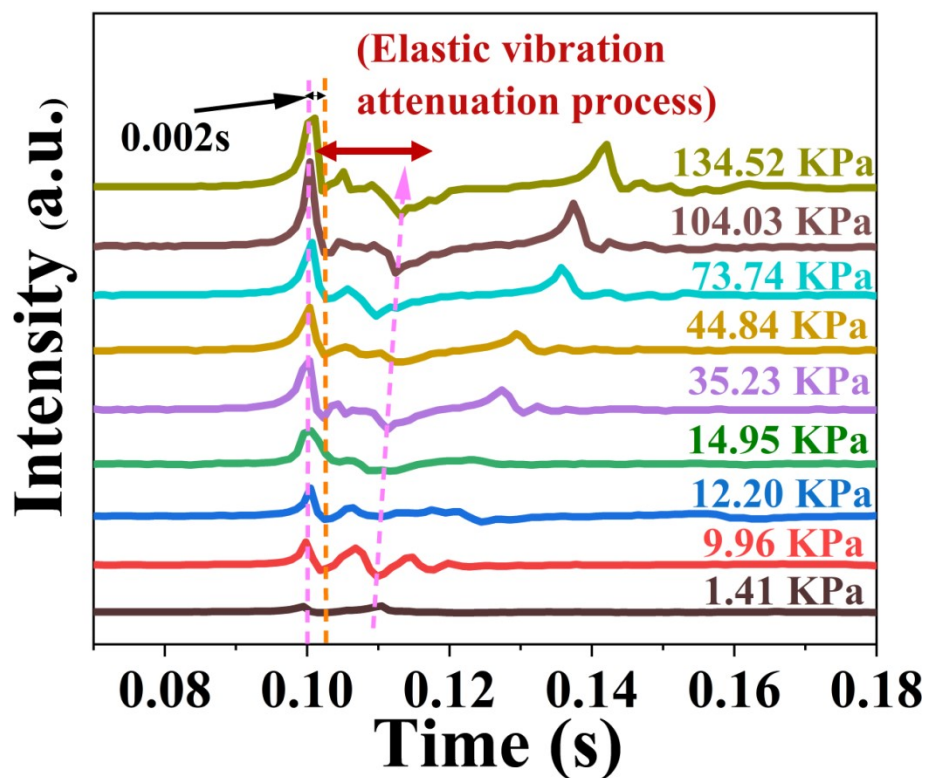Fig. S3. The upper pore structure (a) and bottom barrier layer structure (b) of the AAO template.

Fig. S4. Output performance of the N–TENG device under different external stresses.

Moreover, the time interval between the releasing output and compressing output was approximately 0.002 s (Fig. S3), indicating that it has high sensitivity, laying the foundation for its further application in self-powered sensors. Furthermore, the signal gradually

diminished until it disappeared; accordingly, elastic vibration occurred under the action of a force in the PDMS layer, and the duration of elastic vibration increased gradually with the enhancement of stress. Note that the shape of the curves is different and easy to distinguish, which also indicates that the device's working mechanism is different under different stress levels.
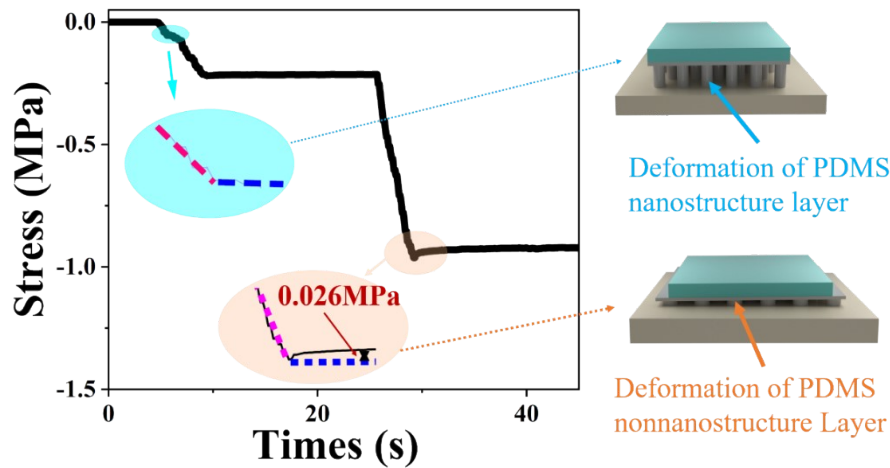

Fig. S5. The relationship between different stresses and times on the surface of the N-TENG device.

To study the deformation mechanism of the specimen under different compressive stresses, we applied different external stresses (0.019, 0.213, 0.957 MPa) to the surface of the N-TENG device. The relationship between time and stress (real stress) on the surface of the N-TENG device was analysed (Fig. S4). To be precise, the creep behaviour of the specimen under different stresses was analysed. When the external stress was 0.019 MPa (no creep behaviour), time had no effect on the real stress, which indicates that PDMS only establishes the compression strain of the nano-structure layer at a lower external stress level. In addition, when the external stress increased to 0.957 MPa (creep behaviour), the true stress gradually decreased to 0.931 MPa with increasing time. Note that with increasing external stress, the creep behaviour became increasingly obvious, meaning that the PDMS deformation of the non-nanostructure increased.
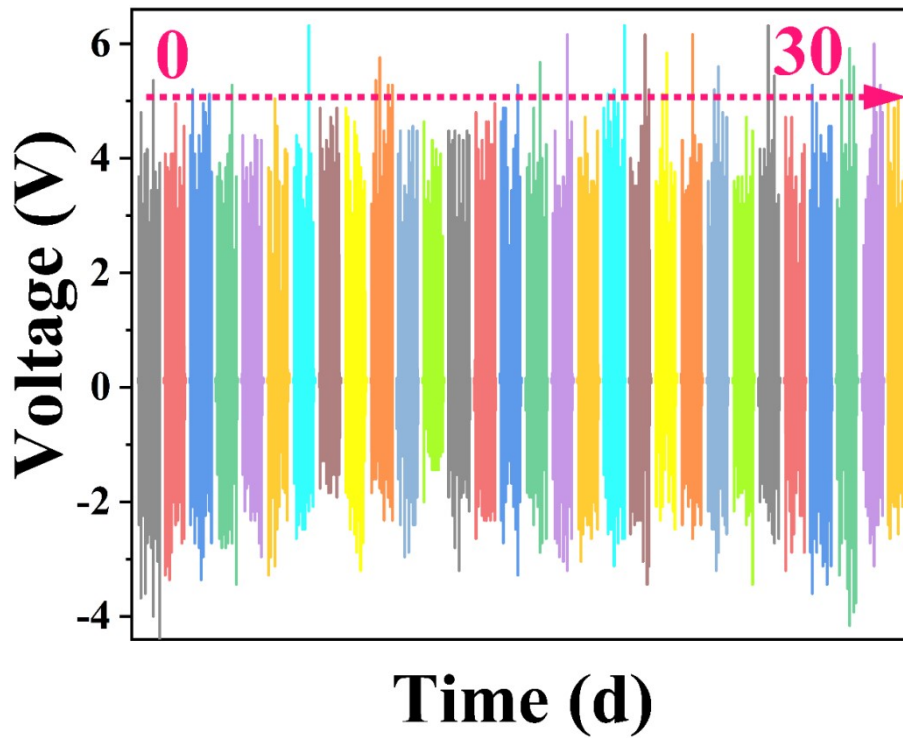
Fig. S6. Stability test of the TENG device.

Note that performance stability is the most important feature of TENG devices in practical applications. [1–5] The output performance of the device did not show any obvious fluctuation or measurable degradation, and the change was negligible, even after 30 d (Fig. S5), which indicates that the manufactured N-TENG device has excellent stability and durability.
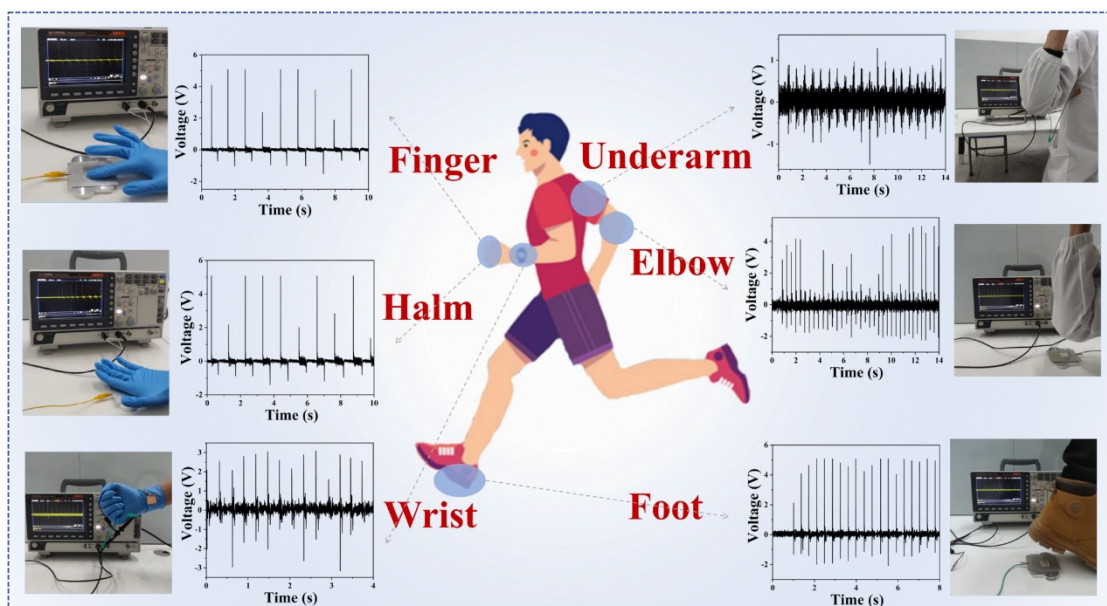
Fig. S7. The development and application of TENG devices. The output voltage signals and test photos of the N-TENG device fixed on various parts of the human body, including fingers, palms, wrists, armpits, elbows, and feet.

The results discussed thus far reveal that the TENG device with a nano-columnar structure was successfully manufactured. As a proof of concept, we demonstrated the possibility of using the N-TENG device as a biomechanical energy collector, which can generate electricity through intense and subtle human movements in daily life. By using the produced TENG equipment, we monitored a series of finger movements, running, arm bending, and arm lifting of self-powered equipment, as shown in Fig. S6. We can see that by fixing the TENG on the fingers, palms, wrists, armpits, elbows and feet, the maximum output V_{oc} was ~5.1, ~5, ~3.0, ~4.4, ~0.8, ~5 and ~5.1 V, respectively (Fig. S6). This result is due to the compression stress applied on the TENG device during human motion. These phenomena show good consistency with the analysis of Eqns. (2)–(6). Therefore, we believe that N-TENG equipment can collect and convert a small amount of mechanical energy.
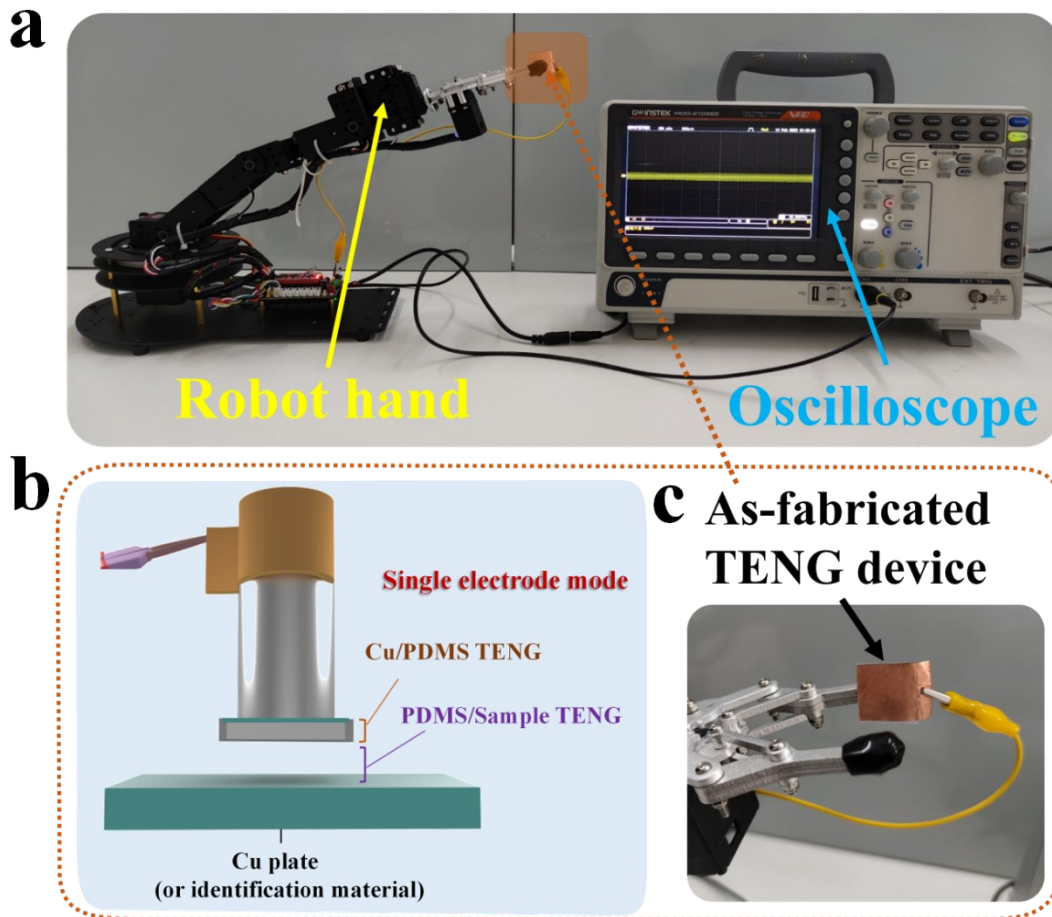
Fig. S8. Schematic diagram for data acquisition. (a, b) Mechanism illustration of data processing and identification and (c) images of the experimental setup using the TENG for accurate recognition.

Output voltage signals are often influenced by a combination of the contact material, contact pressure, and contact environmental conditions. In this work, the height of the object in free fall remained the same (0.04 m), and the mass of the weights was 0.04 kg. The calculated compressive stress on the devices was 5.63 KPa according to Eqns. (1)–(4). The fixed positions of the device and target material are shown in Fig. S7 b. Specifically, two TENG devices, Cu/PDMS (N-TENG) and PDMS/sample, were established, resulting in the formation of two sensing signals from the N-TENG sensor as it contacted different materials. We concluded that various materials provide different electrical signals, accompanied by unique characteristics; hence, the triboelectric signals generated by the as-fabricated TENG are capable of sensitive detection for contact materials. The overview

and ideal experimental images of the involved intelligent tactile sensing system based on the triboelectric signal and deep learning are shown in Fig. S7 a and c. The sensor is fixed on the inside of the manipulator. Extracting characteristics from multiple electrical signals offers exciting opportunities to achieve improved recognition accuracy.[6–8] With the help of machine learning, more deep-rooted features of the identified materials can be captured and eventually achieve accurate identification independent of the environment.[9, 10]
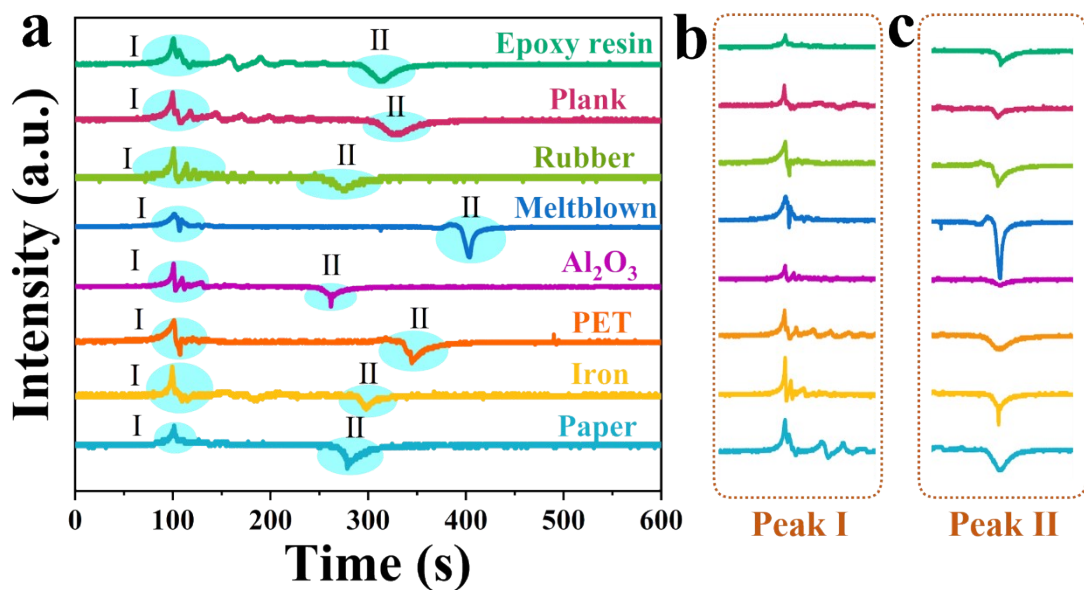

Fig. S9. The sensing signals from the sensor as it contacts different materials (a) and the corresponding partially enlarged diagram (c,d).

In this work, when the TENG struck the material surface, the signal curve from the TENG-based tactile sensor was used to identify unknown and contact materials, as shown in Fig. S8. The signal curve of rubber had only one peak, and all others had two peaks (Fig. S8 b and c). The relative strength of the contact/separation peak was different, and the distance between the two peaks on the curve was also different. According to the analysis in Fig. 3b, two opposite peaks appeared on the signal curve (peak I in Fig. S8 b), which indicate Cu/PDMS contact and separation, respectively, which is consistent with the observation in Fig. 3c. Note that the signal in Fig. S8c was from the PDMS/sample TENG (the corresponding schematic diagram is shown in Fig. S8b), and the contact separation

process between the sample material and the PDMS sensor surface was equivalent to the complete charge transfer process in single-electrode mode. When the two made contact, the charge was separated at the contact interface, resulting in two separated V_{oc} values. Importantly, the presence of alumina reduced the output effect of the device. In Fig. S8a, when the PDMS contacted aluminium, the output voltage was small and not conducive to identification (Fig. 4c). In addition, with the help of the difference in the characteristics of the target object, the above components can further promote the differential characteristics of the PDMS/sample TENG signal. It is important to emphasise that these two guiding effects could lead to different shapes of peaks.
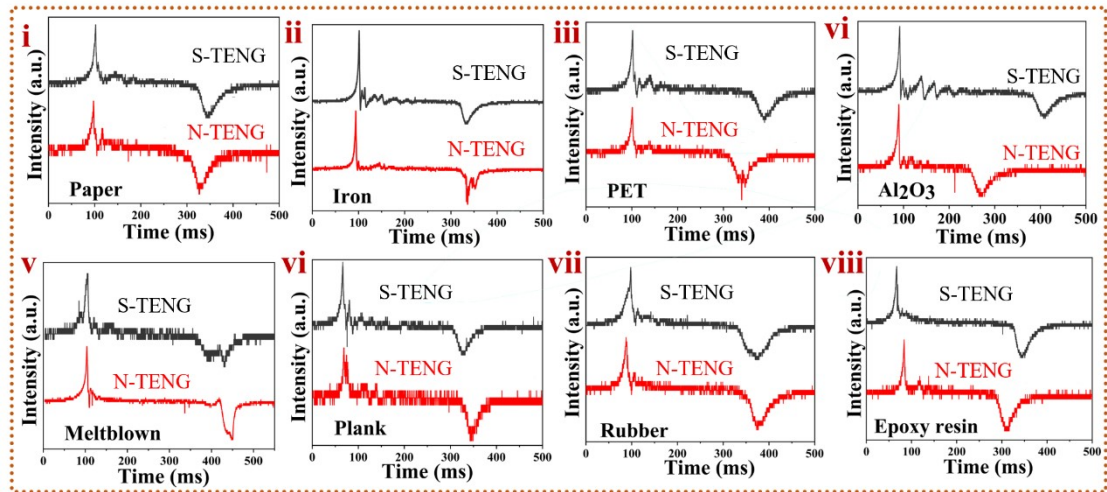
Fig. S10. Typical waveforms of S-TENG and N-TENG sensors when identifying 8 different materials.

To intuitively analyse and compare, we uniformly normalised the data obtained, as shown in Fig. S10. The waveforms of eight different objects show the contact-induced electrification response to the contact release motion. Note that no significant difference was observed between the waveforms of the S-TENG and N-TENG sensors for the five materials of paper, PET, plank, rubber, and epoxy resin (Figs. S10 iiii and vi-viii). In addition, as shown in Fig. S10 ii, the N-TENG had a double peak at the peak II position, that is, the process of releasing a negative charge occurred twice in succession. In Fig. S9 iv, the peak waveforms of the two sensors were significantly different, and the N-TENG released negative charges faster than the S-TENG. Also note that in Fig. S10 v, the obvious difference between the S-TENG and N-TENG waveforms was that the N-TENG had a small opening downwards peak at the position of peak II, releasing a negative charge, which is attributed to the modulus of the material. Based on these results, we concluded that various materials provide different TENG electrical signals, accompanied by unique characteristics. Specifically, the triboelectric signals generated by the as-fabricated N-TENG are capable of sensitive detection of contact materials.
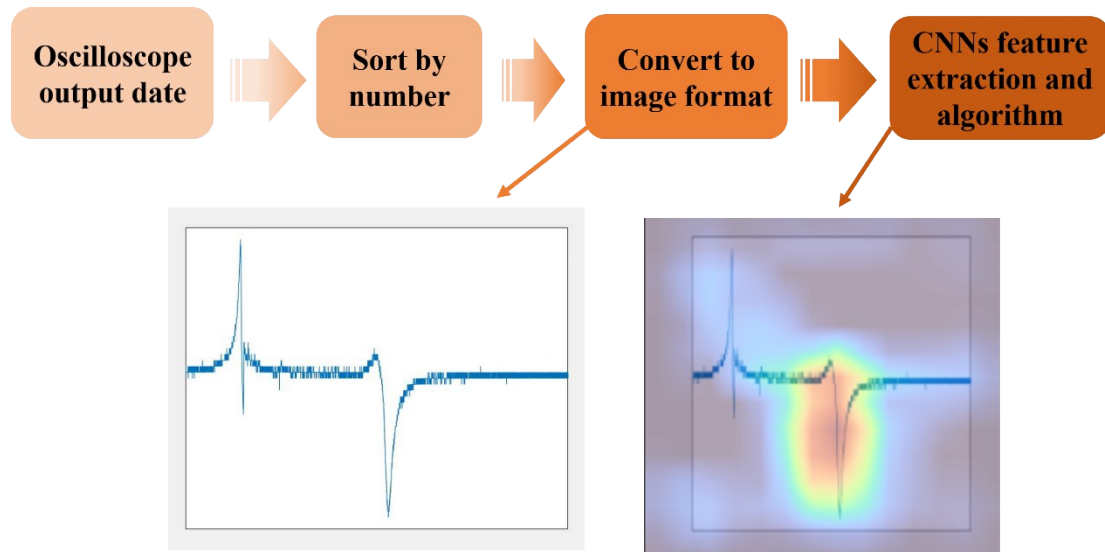
Fig. 11. Workflow of as-fabricated TENG touch sensing.

Fig. S10 displays the workflow of as-fabricated TENG touch sensing. The data from the oscilloscope were numbered and formatted, and the CNN features were extracted and recognised sequentially. Then, we could obtain the recognition result.

REFERENCES

[1] S. Li, Z. Zhao, D. Liu, J. An, Y. Gao, L. Zhou, Y. Li, S. Cui, J. Wang and Z. L. Wang, *Adv. Mater.,* 2022, **34**, e2110363.

[2] S. Fu, W. He, Q. Tang, Z. Wang, W. Liu, Q. Li, C. Shan, L. Long, C. Hu and H. Liu, *Adv. Mater.,* 2022, **34**, e2105882.

[3] J. Li, Y. Long, F. Yang and X. Wang, *Eco Mat.,* 2020, **2**, e12045.

[4] X. Y. Qiu, J. Liu, B. Zhou, X. X. Zhang, *Adv. Funct. Mater.,* 2023, **21**, 2300321.

[5] G. Khandelwal, N.P.M. Joseph Raj, N.R. Alluri and S. J. Kim, *ACS Sustainable Chemistry & Engineering,* 2021, **9**, 9011−9017.

[6] F. Wen, Z. Sun, T. He, Q. Shi, M. Zhu, Z. Zhang, L. Li, T. Zhang and C. Lee, *Adv. Sci.,* 2020, **7**, 2000261.

[7] H. Zhou, D. Li, X. He, X. Hui, H. Guo, C. Hu, X. Mu, Z. L. Wang, *Adv. Sci.* 2021, **8**, e2101020.

[8] M. Zhu, Z. Sun, Z. Zhang, Q.   Shi, T. He, H. Liu, T. Chen, C. Lee, *Sci Adv.* 2020, **6**, eaaz8693.

[9] C. Chen, S. Zhao, C. Pan, Y. Zi, F. Wang, C. Yang, Z. L. Wang, *Nat. Commun.,* 2022, **13**, 1391.

[10] X. Wei, B. Wang, Z. Wu, Z. L. Wang, *Adv. Mater.,* 2022, **34**, e2203073.